Published OnlineFirst April 3, 2015; DOI: 10.1158/0008-5472.CAN-14-2156

Therapeutics, Targets, and Chemical Biology

Cancer Research

Rho Kinase Inhibitors Block Melanoma Cell Migration and Inhibit Metastasis

Amine Sadok[1], Afshan McCarthy[1], John Caldwell[2], Ian Collins[2], Michelle D. Garrett[2], Maggie Yeo[1], Steven Hooper[3], Erik Sahai[3], Sandra Kuemper[1], Faraz K. Mardakheh[1], and Christopher J. Marshall[1]

Abstract

There is an urgent need to identify new therapeutic opportunities for metastatic melanoma. Fragment-based screening has led to the discovery of orally available, ATP-competitive AKT kinase inhibitors, AT13148 and CCT129254. These compounds also inhibit the Rho-kinases ROCK 1 and ROCK 2 and we show they potently inhibit ROCK activity in melanoma cells in culture and *in vivo*. Treatment of melanoma cells with CCT129254 or AT13148 dramatically reduces cell invasion, impairing both "amoeboid-like" and mesenchymal-like modes of invasion in culture. Intravital imaging shows that CCT129254 or AT13148 treatment reduces the motility of melanoma cells *in vivo*. CCT129254 inhibits melanoma metastasis when administered 2 days after orthotopic intradermal injection of the cells, or when treatment starts after metastases have arisen. Mechanistically, our data suggest that inhibition of ROCK reduces the ability of melanoma cells to efficiently colonize the lungs. These results suggest that these novel inhibitors of ROCK may be beneficial in the treatment of metastasis. *Cancer Res; 75(11); 2272–84. ©2015 AACR.*

Introduction

Cancer metastasis is a multistep process that involves migration of tumor cells, local invasion, entry into the circulation, arrest at secondary sites, extravasation, and colonization (1). Many studies implicate the Rho family of small GTPases as key regulators of cell migration (2). Through their actions on the cytoskeleton and actomyosin contractility, the Rho-associated kinases, ROCK1 and ROCK2 (referred to here as ROCK), play a central role in the regulation of cell migration and affect several components of the metastatic process, including migration, local invasion, and cell proliferation (3). ROCK signaling has also been implicated in stiffening of the extracellular matrix, which has been shown to contribute to increased cell proliferation and more aggressive tumor behavior (4, 5). These observations suggest that potent inhibition of ROCK could impair the metastatic process and tumor growth, establishing the kinases as attractive targets for antimetastatic therapies. ROCK1 and ROCK2 belong to the AGC kinase family of serine/threonine protein kinases, which includes PKA and AKT/PKB (6), and are activated by binding to active Rho. Active ROCK phosphorylates several substrates, including LIM domain kinases (LIMK1 and 2), myosin light chain (MLC2), and the myosin-binding subunit (MYPT1) of the myosin phosphatase (7). Thus, ROCK signaling plays a central role in the organization of the actin cytoskeleton, and activates myosin II–dependent contraction of actomyosin fibers, which regulates cell–cell contact and cell migration (3). Single tumor cells can either move in an elongated, protrusive mode or in a rounded, bleb-based fashion often referred to as "amoeboid" movement (8, 9). These two modes of movement are interconvertible and are both dependent on actomyosin contractility. However, rounded, bleb-based movement requires higher levels of actomyosin contractility than the elongated, protrusive mode (10, 11). Although the first generation of ROCK inhibitors, such as Y27632 (12) and H1152 (13), inhibits highly contractile, bleb-based movement, they can convert melanoma cells to elongated, protrusive movement that requires lower levels of actomyosin contractility (8, 10, 11). Consequently, they fail to block cell migration completely. Recent studies reported the development of several new ROCK inhibitors, including, OXA-06 and RKI-18, which showed good potency against ROCK *in vitro* and in cells (14, 15). However, the OXA-06 compound has poor pharmacokinetic properties for use *in vivo* (14) and no *in vivo* data for RKI-18 were reported (15).

In order to identify potent ROCK inhibitors that are active *in vivo*, we have studied the novel ATP-competitive AKT inhibitors CCT129254 and AT13148, which have been developed to have good pharmacokinetic properties *in vivo* and potently inhibit ROCK *in vitro* (16, 17). We have carried out these studies in melanoma cells, because previous work has identified key roles for ROCK signaling in invasion of melanoma cells (11, 18, 19) and we have established an orthotopic model of spontaneous metastasis for assessment of inhibitors *in vivo*. Metastatic melanoma shows considerable genetic heterogeneity with mutations in the proto-oncogenes BRAF and NRAS, and loss of tumor-suppressor genes, including $p16^{INK4}$, $p14^{ARF}$, and PTEN (20, 21).

[1]Division of Cancer Biology, Institute of Cancer Research, London, United Kingdom. [2]Cancer Research UK Cancer Therapeutics Unit, Division of Cancer Therapeutics, Institute of Cancer Research, Sutton, Surrey, United Kingdom. [3]Tumour Cell Biology Laboratory, Cancer Research UK London Research Institute, London, United Kingdom.

Note: Supplementary data for this article are available at Cancer Research Online (http://cancerres.aacrjournals.org/).

Corresponding Authors: Christopher J Marshall, Division of Cancer Biology, Institute of Cancer Research, 237 Fulham Road, London SW3 6JB, United Kingdom. Phone: 44-2071535174; Fax: 44-2073525630; E-mail: chris.marshall@icr.ac.uk; and Amine Sadok, amine.sadok@icr.ac.uk

doi: 10.1158/0008-5472.CAN-14-2156

Published OnlineFirst April 3, 2015; DOI: 10.1158/0008-5472.CAN-14-2156

Despite the considerable progress using targeted therapies against oncogenic BRAF and immunotherapies (22), resistance to therapies invariably develops (20, 23). There is, therefore, a need for additional treatment strategies, including targeting of the metastatic process. We have investigated the effects of ROCK inhibitors CCT129254 and AT13148 on actomyosin contractility and cell movement in tissue culture and *in vivo* to assess effects on melanoma cell movement. Using the orthotopic melanoma metastasis model and an experimental metastasis assay, we show that these agents reduce metastasis and inhibit cell proliferation, suggesting that inhibition of ROCK in melanoma could be beneficial in the treatment of metastasis.

Materials and Methods

Cell lines, treatments, and reagents

A375p and A375M2 human $BRAF^{V600E}$ melanoma cells were from R. Hynes (Howard Hughes Medical Institute, Massachusetts Institute of Technology, Cambridge, MA). Human melanoma cells WM266.4, and WM1361 were from R. Marais (Paterson Institute, Manchester, United Kingdom). All these cell lines were authenticated by STR profiling by LGC standards on June 2014. 4599 and 690cl2 cells were generated by N. Dhomen and R. Marais (Paterson Institute) from tumors arising in the $Braf^{V600E}$ mouse model (24) and from tumors arising from the $Braf^{V600E}$; $Pten^{fl/fl}$ mouse melanoma tumor model, respectively. The ROCK-deficient melanoma cell lines used in this study were generated from tumors arising in mice carrying $Braf^{V600E}$; $Pten^{fl/fl}$; $Rock1^{F6/wt}$; $Rock2^{F5\text{-}6/F5\text{-}6}$, *Tyr-CreERT2* after induction by tamoxifen treatment. Mouse embryonic fibroblasts (MEF) were derived from embryos carrying conditionally targeted alleles of *Rock1* and *Rock2* (S. Kuemper, A. McCarthy, and C.J. Marshall; manuscript in preparation), where loxP sites flank exon 6 of *Rock1* ($Rock1^{F6}$) and exons 5–6 of *Rock2* ($Rock2^{F5\text{-}6}$). These cells were transformed by infection with retrovirus pBABE-p53DD followed by pBABE-$HRas^{V12}$ (Addgene plasmids #1768, #9058, respectively); recombined *Rock* alleles were generated by infection with Adeno Cre (Gene Transfer Vector Core, University of Iowa, Iowa City, IA) to generate $Rock1^{\Delta F6/\Delta F6}$;$Rock2^{\Delta F(5\text{-}6)/\Delta F(5\text{-}6)}$. Control cells ($Rock1^{F6/F6}$;$Rock2^{F(5\text{-}6)/F(5\text{-}6)}$) were generated by infection of the transformed MEFs with Adeno GFP. CCT129254, CCT130293 (16), and AT13148 (17) were synthesized in-house. MK2206 was obtained from ChemieTek, H1152 from MERCK Millipore, and Y27632 from Tocris Bioscience. Rabbit anti-phospho MLC2 (Thr18/Ser19), rabbit anti-phospho PRAS40 clone (C77D7), rabbit anti-phospho AKT (Ser473) clone (D9E), rabbit anti-total PRAS40 clone (D23C7), and mouse anti-total AKT clone (40D4) antibodies are from Cell Signaling Technology. Mouse anti-MRCL3/MRLC2/MYL9 clone (E-4) is from Santa Cruz Biotechnology.

Gel contraction assay

A total of 10^6 melanoma cells were embedded in 500 μL of a 2.3 mg/mL collagen-I gel and plated in a 24-well plate. After the gel was set at 37°C for 1 hour, 500 μL of media, containing inhibitors or vehicle, was added on top of the gel. After 24 hours, the plates were scanned and the diameter of the gel and well was measured using the ImageJ software. The extent of contraction was assessed by subtracting the gel area from the well area. For each well, we calculated the percentage of gel contraction using the formula $100 - [(\text{area of the gel/area of an empty well}) \times 100$; ref. 19].

3D-invasion assay

Cells were suspended in 2.3 mg/mL of serum-free liquid bovine collagen at 10^5 cells/mL. Hundred-microliter/aliquots were dispensed into black 96-well ViewPlates (PerkinElmer) coated with bovine serum albumin. Plates were centrifuged at 300 × *g* and incubated in a 37°C/10% CO_2 tissue culture incubator. Once collagen had polymerized, serum-depleted medium with either drugs or vehicle was added on top of the collagen. After 24-hour incubation at 37°C in 10% CO_2, cells were fixed and stained for 4 hours in 4% formaldehyde solution (Sigma-Aldrich) containing 5 μg/mL Hoechst 33258 nuclear stain (Invitrogen). The plates were then imaged by Operetta High Content Imaging System (PerkinElmer) using Z-planes at 0, 30, and 60 μm. Nuclear staining was quantified by the Harmony software package (PerkinElmer) at each plane. The invasion index was calculated as the sum of the number of cells at 30 and 60 μm, divided by the total number of cells. Samples were run in quadruplicate and averaged. Data were expressed as mean from three independent experiments.

Western blot

Cells were seeded on plastic 6-well plates at a density of 5×10^5 cells per well and allowed to adhere for 2 hours, then serum starved for 16 hours and further treated with inhibitors for the indicated times. Cells were lysed in SDS loading buffer (50 mmol/L Tris pH 6.8, 10% glycerol, 2% SDS, 100 mmol/L dithiothreitol) and boiled for 10 minutes. Cell lysates were resolved by SDS-PAGE, and transferred to PVDF-FL membranes (Millipore). Membranes were incubated with indicated antibodies and visualized by fluorescently conjugated secondary antibodies using the Odyssey Infrared Imaging System (LI-COR). Quantification of the Western blot analyses was operated by LI-COR software (Image studio lite Ver3.1).

Time-lapse microscopy

Cells were seeded on top of 1.7 mg/mL collagen-I gel in medium containing 10% serum and allowed to adhere for 2 hours then medium was changed to 0% serum with inhibitor or vehicle. Imaging started 16 hours after treatment for a further 24 to 40 hours.

Intravital imaging

Nude mice were injected subcutaneously with A375M2 human melanoma cells expressing GFP-LifeAct. Tumors were imaged when they reached 3 to 7 mm. Five mice in each group were dosed with drug twice: once 24 hours before imaging and again 2 hours before imaging. Doses of 200 mg/kg for CCT129254 and 40 mg/kg for AT13148 were used for treatments. Imaging was performed as previously described (25).

Orthotopic melanoma metastasis assay

All animal procedures were approved by the Animal Ethics Committee of the Institute of Cancer Research in accordance with National Home Office regulations under the Animals (Scientific Procedures) Act 1986. 4599 mouse melanoma cells (2×10^5 cells) were injected intradermally into the lateral flanks of 6- to 8-week-old female NOD.Cg-Prkdcscid Il2 rgtm1Wjl/SzJ (NSG) mice; 2 days after injection, the mice were randomly divided into two groups, one group was treated with vehicle only and the other with the drug. CCT129254 was administered at 200 mg/kg in 10% DMSO, 5% Tween 20 in saline, p.o., CCT130293 was administered at 20 mg/kg in 10% DMSO, 1% Tween 20 in saline, i.p., the

Published OnlineFirst April 3, 2015; DOI: 10.1158/0008-5472.CAN-14-2156

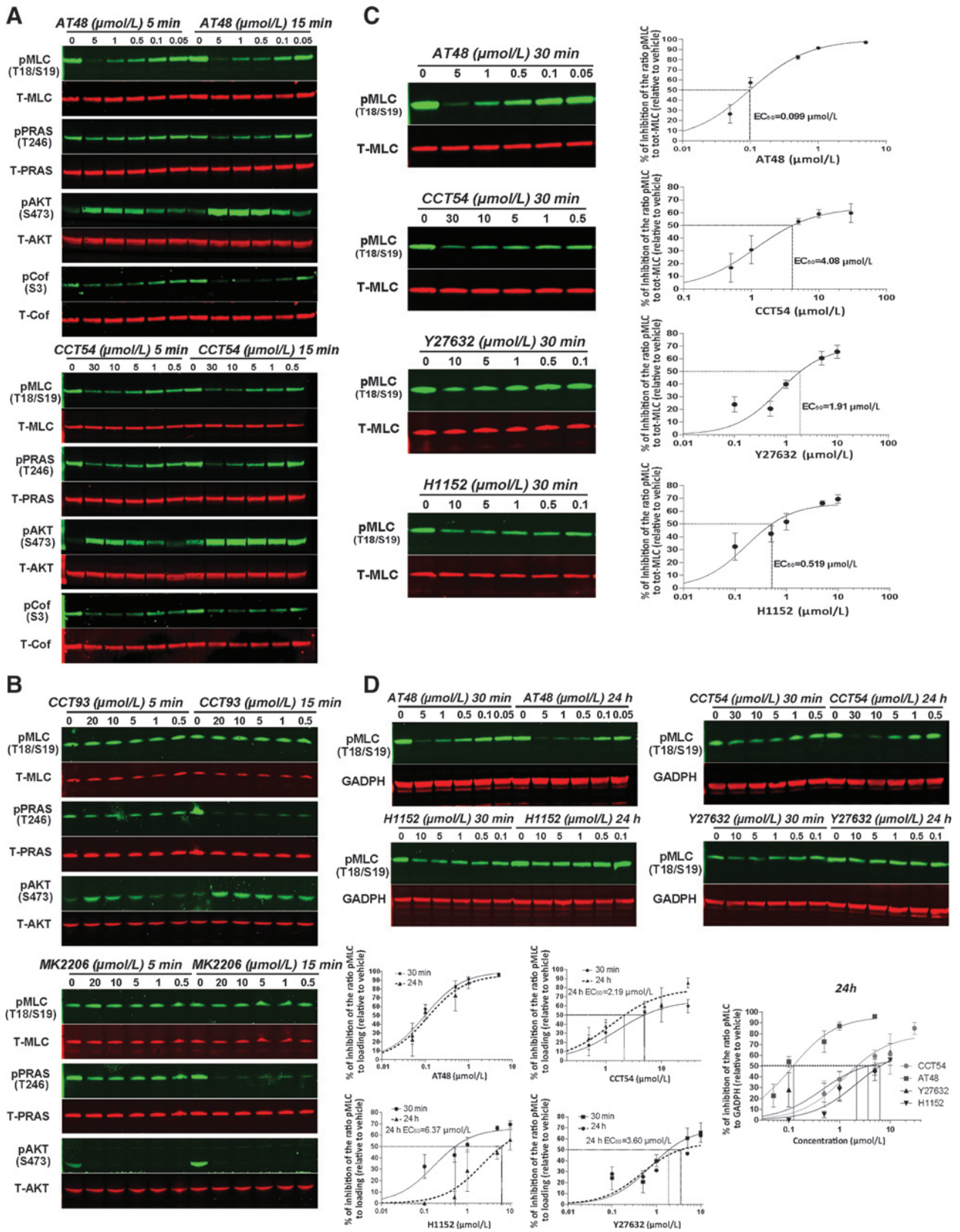

Published OnlineFirst April 3, 2015; DOI: 10.1158/0008-5472.CAN-14-2156

dosing schedule for both drugs was 5 to 7 days. At the end of the experiment, lungs and tumors were excised and fixed in 4% buffered formalin overnight; macroscopic metastases were counted in the lungs using a dissecting microscope. Primary tumors and lungs were embedded in paraffin, gross morphology was assessed on H&E-stained sections. IHC for Ki67 was performed using anti-Ki67 (1:300; Abcam; ab16667). In the lungs, Ki67-positive cells were counted in five individual metastases and in the case of the primary tumors Ki67-positive cells were counted in five fields of view per tumor at a magnification of ×400.

Experimental metastasis assays

Extravasation assay. 4599 melanoma cells were labeled with either Cell Tracker orange (CMRA) at 5 μmol/L or Cell Tracker green (CMFDA) at 1 μmol/L and pretreated with either vehicle, CCT129254 (40 μmol/L), or CCT130293 (10 μmol/L) for 40 hours. The cells were mixed at a ratio of 1:1 with their respective vehicle-treated control and 1×10^6 cells were injected into the tail vein of CD1 athymic mice. The mice were culled 2 and 24 hours after injection, the lungs were perfused with 5-mL PBS as described in Malanchi and colleagues (26), excised and fixed in 4% buffered formalin overnight. Fluorescent images were collected using the Zeiss LSM 710 confocal microscope and the number of green and orange cells was quantified in 12 fields of view per lung at a magnification of ×200.

Lung colonization assay. 4599 melanoma cells expressing luciferase were pretreated with either CCT129254 (40 μmol/L) or CCT130293 (10 μmol/L) for 40 hours; 1×10^6 cells were injected into the tail vein of CD1 athymic mice. Twenty-four days after injection, the mice were subjected to *ex vivo* bioluminescence imaging using the IVIS Lumina II (Xenogen Corporation); luminescence was quantified using Living Image software (Xenogen Corporation). The lungs were fixed in 4% buffered formalin overnight, embedded in paraffin, and IHC for Ki67 was performed as described previously.

Statistical analysis

P values were generated using ANOVA in Figs. 4B and C and 5B and C. For the scatter plot in Fig. 3B, the Mann–Whitney *U* test was used. For all remaining quantifications, the Student *t* test was performed. Unless otherwise stated, error bars indicate SD.

Results

CCT129254 and AT13148 are potent inhibitors of ROCK-driven actomyosin contractility

Fragment-based screening together with medicinal chemistry has led to the discovery and development of compounds targeting AKT/PKB, including the orally available, ATP-competitive kinase inhibitors AT13148 and CCT129254 (16, 17, 27). *In vitro* screening of AT13148 against a panel of kinases shows that it is a multi-AGC kinase inhibitor, with potent activities against ROCK1 (IC_{50} = 6 nmol/L), ROCK2 (IC_{50} = 4 nmol/L), and AKT1, 2, and 3 with IC_{50} values of 38, 402, and 50 nmol/L, respectively (17). CCT129254 inhibits ROCK1 and ROCK2 (IC_{50} = 214 nmol/L and 141 nmol/L, respectively) and AKT2 (IC_{50} = 2.2 nmol/L; ref. 16). Screening against MRCK (myotonic dystrophy kinase-related Cdc42-binding kinase)-α and -β showed that both compounds exhibit very low potency toward MRCK-α (IC_{50} = 1,510 nmol/L and 33,000 nmol/L for AT13148 and CCT129254, respectively) and MRCK-β (IC_{50} = 1,140 nmol/L and 33,000 nmol/L for AT13148 and CCT129254, respectively). Compound CCT130293, which was developed from the same chemical series as CCT129254, also inhibits AKT (IC_{50} = 5 nmol/L), but exhibits very low potency toward ROCK (IC_{50} = 5,788 nmol/L). Further *in vitro* screening of CCT129254, AT13148, and CCT130293 against a panel of 140 kinases revealed that several AGC kinases are commonly inhibited (>70% inhibition) by 1 μmol/L of CCT130293 and either of AT13148 (1 μmol/L) or CCT129254 (1 μmol/L), including PKA, AKT, p70S6K, RSK1/2, PRK, and MSK (Supplementary Table S1). Thus, the pair of inhibitors CCT129254 and CCT130293 provides a set of tools to dissociate between the ROCK-dependent and ROCK-independent signaling.

Using MLC2 phosphorylation at Thr18 and Ser19, a well substantiated read out for ROCK activity in cells (3, 7), we show that 5-minute treatment of 4599 mouse melanoma cells with either CCT129254 or AT13148 potently inhibits phosphorylation of MLC2 in a dose-dependent fashion (Fig. 1A). As expected from previous work (16, 17), CCT129254 and AT13148 strongly inhibited AKT downstream signaling as shown by the decrease in Thr246 phosphorylation of the proline-rich Akt-substrate (PRAS40). The potency of both compounds toward the inhibition of MLC2 phosphorylation is independent from effects on AKT-regulated signaling, as CCT130293, an ATP-competitive inhibitor of AKT that does not inhibit ROCK, and MK-2206, an allosteric inhibitor of AKT, strongly inhibit AKT activity and AKT-downstream signaling but have no effect on phosphorylation of MLC2 (Fig. 1B). The ATP-competitive AKT inhibitors CCT129254, CCT130293, and AT13148 increased Ser473 AKT phosphorylation through stabilization of the ligand-bound phosphorylated protein to dephosphorylation (28), in contrast to the allosteric AKT inhibitor, which inhibits PI3K-dependent phosphorylation of AKT on Ser473 (29). Phosphorylation of MLC2 can also be triggered in cells by the MRCKs-α and -β (10). However, CCT129254 and AT13148 exhibit very low potency toward MRCK-α (IC_{50} = 1,510 nmol/L and 33,000 nmol/L for AT13148 and CCT129254, respectively) and MRCK-β (IC_{50} = 1,140 nmol/L and 33,000 nmol/L for AT13148 and CCT129254, respectively), indicating that the potency of the compounds toward the

Figure 1.
CCT129254 and AT13148 potently inhibit ROCK-dependent phosphorylation of MLC2. 4599 mouse melanoma cells were allowed to adhere for 2 hours, then serum-starved for 16 hours and further treated with the indicated doses of AT13148 (AT48; A, top), CCT129254 (CCT54; A, bottom), CCT130293 (CCT93; B, top), and MK2206 (B, bottom) for either 5 or 15 minutes and then immunoblotted. C, 4599 melanoma cells seeded as in A and treated with the indicated doses of CCT129254, AT13148, H1152, or Y27632 for 30 minutes, and immunoblotted. Quantifications represent the percentage of inhibition (relative to vehicle-treated condition) of the ratio of the pMLC2 fluorescence signal to total MLC2. Mean ± SD for each concentration; $n = 3$ independent experiments. D, melanoma cells were seeded as in C, then treated for 24 hours with the indicated doses of CCT129254, AT13148, H1152, or Y27632 and then immunoblotted for phosphorylatedMLC2 and GADPH. Quantifications are as in C. Mean ± SD for each concentration; $n = 3$ independent experiments. For visualization purposes, 24-hour quantifications for all four inhibitor were assembled in the same graphic (far right).

Published OnlineFirst April 3, 2015; DOI: 10.1158/0008-5472.CAN-14-2156

inhibition of MLC2 phosphorylation is mediated by their effect on ROCK. The on-target efficiency of the compounds was further confirmed by the dose-dependent decrease in phosphorylation of LIMK-substrate cofilin, a well-established target of ROCK-dependent signaling (Fig. 1A).

In order to benchmark CCT129254 and AT13148 to that of the prototypical ROCK inhibitors Y27632 and H1152 (12, 13), we measured the level of inhibition of MLC2 phosphorylation in 4599 melanoma cells after 30 minutes of treatment with various concentrations of CCT129254, AT13148, Y27632, and H1152 and determined their respective EC50s (Fig. 1C). We show that AT13148 is the most potent inhibitor of ROCK (EC_{50} = 0.1 μmol/L) followed by H1152 (EC_{50} = 0.5 μmol/L), then Y27632 (EC_{50} = 1.9 μmol/L) and CCT129254 (EC_{50} = 4 μmol/L; Fig. 1C). We next sought to assess the sustainability of ROCK inhibition by each of the compound by determining their 24 hour-EC50s. Results presented in Fig. 1D show that inhibition of ROCK by AT13148 is stable over 24 hours (24-hour EC50 = 0.1 μmol/L), whereas both Y27632- and H1152 dose–response curves exhibited a shift toward lower potency after 24 hours of treatment (24-hour EC50 of 3.6 μmol/L and 6.4 μmol/L, respectively). In contrast, CCT129254 dose–response curve was shifted toward a higher potency after 24 hours of treatment (24-hour EC50 = 2.2 μmol/L), showing the higher stability of CCT129254 and AT13148 over time (Fig. 1D). In order to strengthen the observation that CCT129254 and AT13148 are potent inhibitors of ROCK-driven actomyosin contractility, we assessed their effect on cell-induced contraction of collagen lattices (30). Results presented in Fig. 2A show that CCT129254 and AT13148 are as good as or better inhibitors of collagen contraction in both 4599

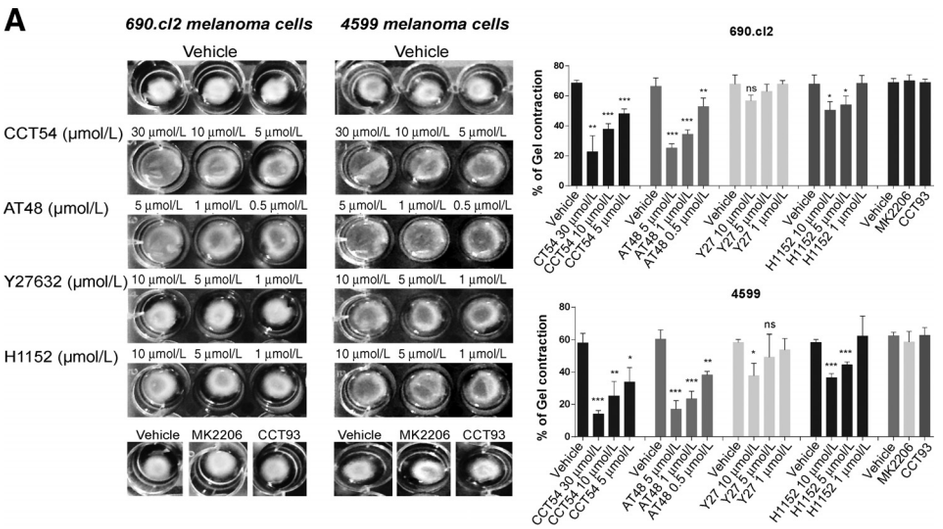

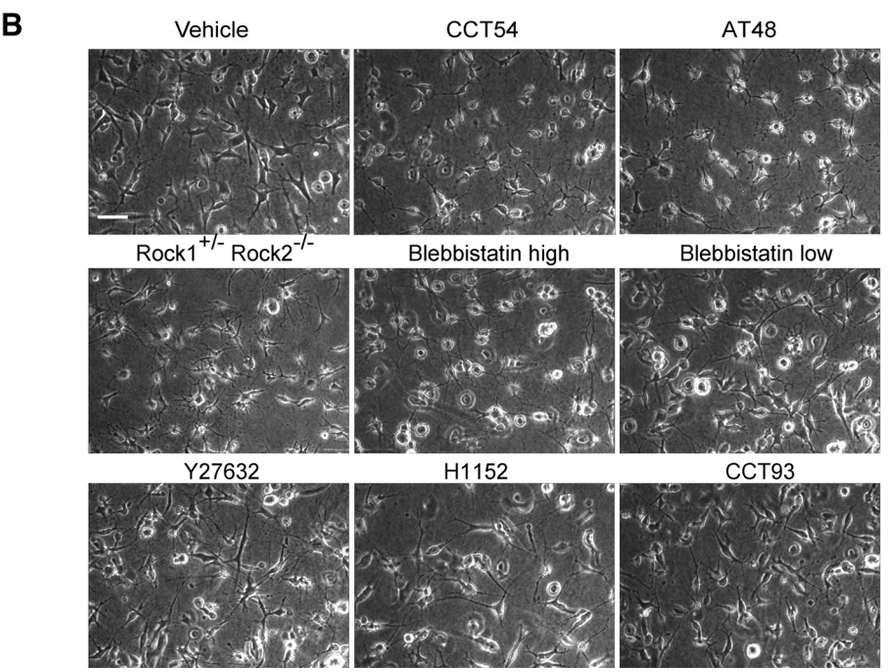

Figure 2.
CCT129254 and AT13148 inhibit actomyosin contractility and induce a collapsed morphology. A, images show gel contraction of 690 and 4599 melanoma cells after 24-hour treatment with 1 μmol/L of MK2206 or 5 μmol/L CCT93 or the indicated doses of CCT129254, AT13148, H1152, or Y27632. Histograms show mean ± SD from $n = 3$ independent experiments. *, $P < 0.05$; **, $P < 0.01$; ***, $P < 0.001$, unpaired t test. B, 690 melanoma cells were seeded on collagen-I gel, then treated in serum-starved condition with CCT54 (10 μmol/L), AT48 (5 μmol/L), Y27632 (10 μmol/L), H1152 (5 μmol/L), blebbistatin low (2.5 μmol/L), and blebbistatin high (25 μmol/L) for 24 hours, then imaged. Genetically deleted ROCK melanoma cells were imaged in the same experimental setting. Bar, 50 μm.

Published OnlineFirst April 3, 2015; DOI: 10.1158/0008-5472.CAN-14-2156

and 690 melanoma cell lines than Y27632 and H1152. The selected concentrations for both compounds exhibited a marginal effect on the viability of 4599 and 690 melanoma cells (Supplementary Fig. S1). Figure 2A also shows that reduction in contractility is independent of inhibition of the AKT-mediated signaling, as inhibition of AKT activity by either MK2206 or CCT130293 has no impact on melanoma cells-mediated gel contraction.

Potent inhibition of ROCK by CCT129254 and AT13148 induces cytoskeletal collapse and reduces cell movement both *in vitro* and *in vivo*

Actomyosin contractility is essential for the maintenance of cell shape; partial inhibition of actomyosin contractility through treatment with low doses of the myosin II ATPase inhibitor blebbistatin (31) leads to an increased number of protrusions in cells with an elongated, protrusive morphology (Fig. 2B). However, strong inhibition of actomyosin contractility resulting from treatment with high doses of blebbistatin (25 μmol/L) leads to a collapsed morphology with a round cell body and multiple, highly dynamic protrusions (Fig. 2B; ref. 10). Treatment of 690 melanoma cells with CCT129254 (10 μmol/L) or AT13148 (1 μmol/L), or a high dose of blebbistatin (25 μmol/L), led to a collapsed morphology (Fig. 2B and Supplementary Movies S1–S3), which was also seen in other melanoma cell lines (not shown). However, treatment with Y27632 (10 μmol/L) or H1152 (5 μmol/L) led to an increase in the length of protrusions similar to a low dose of blebbistatin (2.5 μmol/L) rather than a collapsed morphology. Thus, treatment with CCT129254 or AT13148, but not Y27632 or H1152, mimics the action of complete inhibition of myosin II by blebbistatin. Importantly, the collapsed morphology induced by CCT129254 or AT13148 treatment was also seen following genetic deletion of *Rock1* and *Rock2*, because cells derived from a mouse model of melanoma with *Pten* deletion and $Braf^{V600E}$ mutation, with loss of three alleles of *Rock* (S. Kuemper, A. McCarthy, and C.J. Marshall; manuscript in preparation) also exhibited a collapsed morphology when cultured on top of a thick collagen-I gel (Fig. 2B). In contrast, CCT130293 that inhibit AKT, but not ROCK, did not cause a collapsed morphology (Fig. 2B). Taken together, these results confirm that the dramatic effect of CCT129254 and AT13148 on actomyosin contractility and melanoma cell morphology is mainly due to their potency as inhibitors of ROCK.

Treatment with ROCK inhibitors Y276352 or H1152 induces a switch from a highly contractile-bleb based, rounded, amoeboid-like movement to a low contractile, elongated, protrusive mesenchymal-like mode of migration (9, 32, 33). Inhibition of both types of cell movement by ROCK inhibitors alone has so far been unsuccessful. Furthermore, there are reports showing that treatment with Y276352 or H1152 can enhance protrusive mesenchymal-like cell migration (8, 11). Because our studies show that CCT129254 and AT13148 are more potent than Y276352 and H1152 in sustaining high level of inhibition of MLC2 phosphorylation, we tested the efficacy of the compounds on the inhibition of different modes of cell movement in tissue culture. We selected a panel of cell lines with different genetic backgrounds and different migratory behavior in a 3D environment and subjected them to assays of invasion into collagen-I gels that is permissive for both rounded, amoeboid-like movement and elongated, protrusive movement (8, 11). 4599 mouse melanoma cells and WM1361 human melanoma cells mainly move with a rounded morphology in a soft 3D collagen-I matrix, whereas 690 mouse melanoma cells exhibit an elongated morphology. WM2664 human melanoma cells invade as a mixture of rounded and elongated cells (11, 34). CCT129254 or AT13148 treatments consistently inhibit all modes of invasion in a dose-dependent way; irrespective of the genetic background of the tested melanoma cell line (Fig. 3A), whereas Y276352 and H1152 had variable effects. This finding demonstrates that ROCK activity is needed for both amoeboid and elongated modes of movement. Importantly, neither CCT130293 nor MK-2206 affected melanoma cell invasion in collagen-I (Fig. 3A), arguing that inhibition of AKT is not responsible for the block in invasion.

To investigate whether CCT129254 or AT13148 inhibited melanoma cell movement *in vivo*, we used intravital imaging of GFP-LifeAct-expressing A375M2 melanoma cells, which have been shown to use amoeboid, rounded movement, and elongated protrusive movement *in vivo* (35), in CCT129254- or AT13148-treated athymic mice. Figure 3B shows that tumor cell movement is consistently impaired upon treatment with the compounds (Fig. 3B). Taken together, these results show that potent inhibition of ROCK, by either CCT129254 or AT13148, decreases melanoma cell motility both *in vitro* and *in vivo*.

Inhibition of melanoma metastasis by CCT129254

In order to assess the effect of the compounds on spontaneous melanoma metastasis, we set up an orthotopic assay of melanoma metastasis that recapitulates all the steps of metastasis (invasion, intravasation, survival in blood stream, extravasation, and growth at the secondary site) rather than the more limited assay of experimental metastasis by tail vein injection that only evaluates survival in blood stream, extravasation, and growth at the secondary site. Suspensions of 2×10^5 melanoma cells were injected into the dermis of immune-deficient NOD *scid* gamma (NSG) mice, and macroscopic lung metastases scored 24 days later. The 4599 mouse melanoma cells (24, 36) generated a consistently high number of lung metastases (50 ± 10 foci/lung) in this experimental setting. First, we used a schedule of treatment where 2 days after intradermal injection of 4599 melanoma cells, CCT129254, CCT130293, or vehicle were administered using cycles of 5 days treatments/2 days of rest; the size of the primary tumor were monitored for 24 days. After 24 days, the lungs were collected and macroscopic metastases scored (Fig. 4A). In this experimental setting, both compounds significantly slow down the growth of the primary tumor (Fig. 4B and C) and both treatments led to a decrease in the number of macroscopic metastases (Fig. 4D and E). Because in this treatment regime growth of the primary tumor is affected, it is difficult to separate effects on metastasis from effects on growth of the primary tumor. However, we found that a discontinuous schedule where 2 weeks of drug treatment are followed by a 10-day treatment-free period has smaller effects on primary tumor growth (Fig. 4G and H). With this treatment schedule CCT130293 treatment did not affect the number of macroscopic metastases (Fig. 4I), whereas CCT129254 treatment led to a strong decrease in the number of metastases, with a marginal effect on the growth of the primary tumor (Fig. 4I). This suggests that the CCT129254-mediated decrease in metastasis is not solely the consequence of inhibition of tumor growth at the primary site. We next sought to test the ability of CCT129254 to reduce the progression of the disease in a more clinically relevant setting where treatment starts after metastasis has been established. In this setting, treatment starts 15 days after intradermal injection of the cells and lasts for a further 15

Published OnlineFirst April 3, 2015; DOI: 10.1158/0008-5472.CAN-14-2156

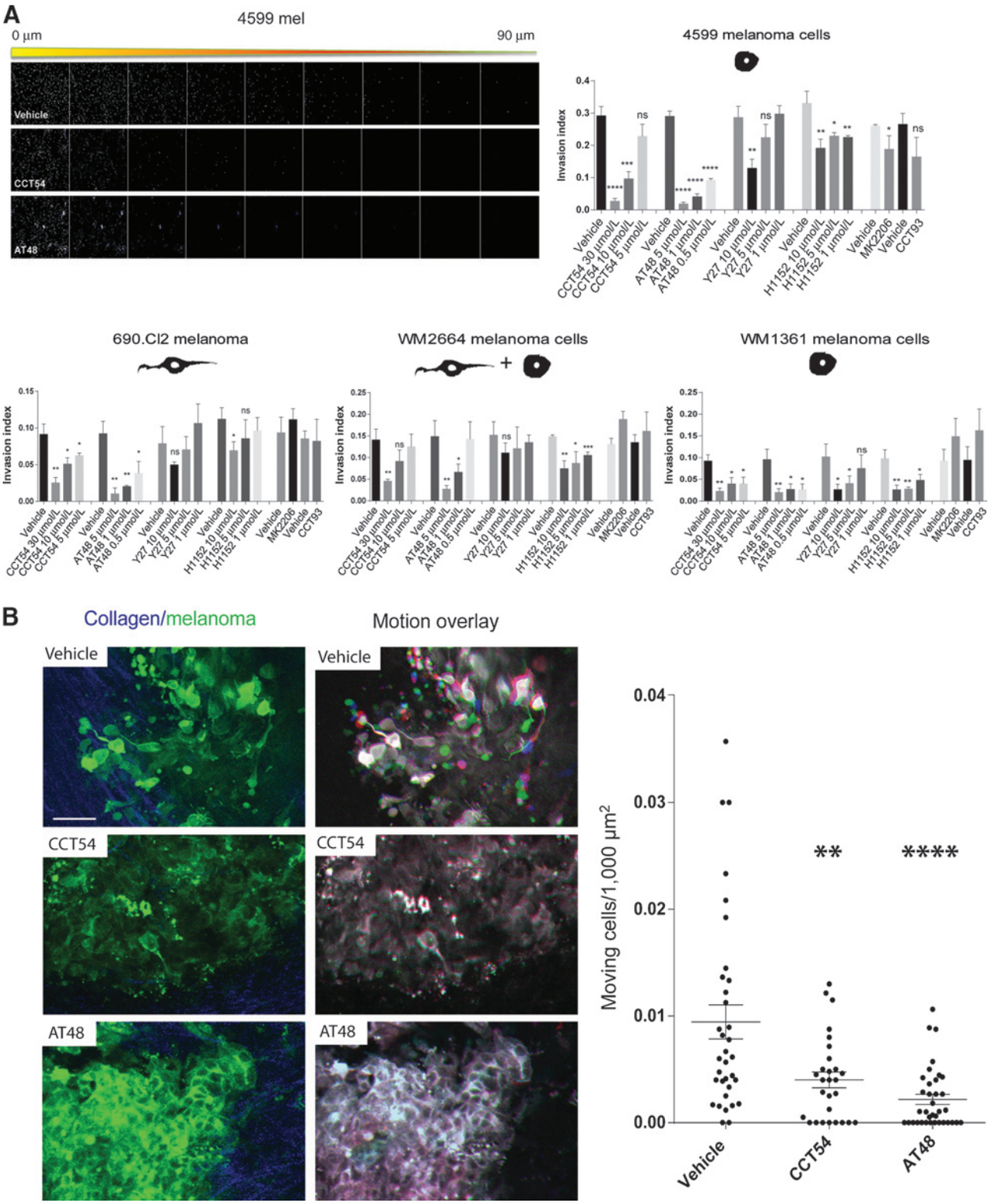

Figure 3.
CCT129254 and AT13148 inhibit all types of movement *in vitro* and *in vivo*. A, human and mouse melanoma cells exhibiting different modes of movement in 3D were assessed for invasion in collagen-I, in the absence or presence of 1 μmol/L of MK2206 or 5 μmol/L CCT93 or the indicated doses of CCT129254, AT13148, H1152, or Y27632. Representative images of invasive 4599 melanoma cells treated with either 30 μmol/L of CCT54 or 5 μmol/L of AT48 present between 0 and 90 μm. (*Continued on the following page.*)

Published OnlineFirst April 3, 2015; DOI: 10.1158/0008-5472.CAN-14-2156

days, at the end of which lungs were collected and the number of macroscopic metastases scored (Fig. 5A). We show that although both CCT129254 and CCT130293 treatments slightly reduced the growth of the tumor at the primary site (Fig. 5B and C), only CCT129254 treatment consistently decreased the number of macroscopic metastases (Fig. 5D and E). We showed, through analyzing Ki67 staining that CCT129254 treatment, but not CCT130293 treatment, induced a decrease in the number of proliferating cells in the metastases, suggesting that a part of the mechanism of action of CCT129254 involves the inhibition of metastatic cell proliferation (Fig. 5F and G). In order to confirm that ROCK and AKT are inhibited *in vivo*, we carried out a pharmacodynamic study of CCT129254 and CCT130293. Supplementary Fig. S2 shows that in tumors from treated mice, CCT129254 inhibits both ROCK, as shown by decreased phosphorylation of MLC2, and AKT as shown by decreased phosphorylation of PRAS and increased phosphorylation of Ser473 of AKT (28), whereas CCT130293 only inhibits AKT activity.

Previously reported pharmacokinetic and pharmacodynamic analysis of AT13148 has established an orally administrated dose of 40 mg/kg as the optimal, therapeutically active concentration in male athymic mice (17). Although we could show a consistent impairment of the motility of melanoma tumor cells in culture and *in vivo* (Fig. 3B), as well as an impairment of primary tumor growth (Supplementary Fig. S3) in nude mice, we experienced high toxicity when using AT13148 in the heavily immuncompromised NSG mice required for the spontaneous metastasis assay. Therefore, in order to avoid toxicity-driven issues, we did not pursue AT13148 in further studies on metastasis and focused on CCT129254.

ROCK inhibition decreases outgrowth of melanoma cells in the lung

We have shown that treatment with CCT129254 inhibits proliferation at the metastatic site. However, as metastasis is a multistep process, we sought to determine whether other steps during metastasis are affected by CCT129254. Efficient colonization of the lung parenchyma and the subsequent formation of macrometastases involves survival in the blood stream, entry into the lung, survival, and proliferation in the new, "hostile" environment (1). In order to test whether the survival in the blood stream and extravasation are affected by CCT129254 treatment, we performed an assay in which we transiently labeled 4599 melanoma cells with either orange CMRA or green CMFDA CellTracker dyes and then treated the orange or green labeled cells for 40 hours with the inhibitors or vehicle. Treated cells and their differently labeled controls were then mixed 1:1 and injected into the tail vein of athymic mice. Lungs were collected at 2 and 24 hours after injection and scored for the number of orange and green cells. Importantly, neither CCT129254 nor CCT130293 treatments affected the survival of the melanoma cells in the blood stream or their extravasation potential as the same number of compound-treated and vehicle-treated cells were lodged in the lungs 2 hours after the injection (Fig. 6A). Drug treatment did not increase the clearance of the melanoma cells from the lungs as the same number of inhibitor-treated and vehicle-treated cells remained 24 hours after injection (Fig. 6A). Similarly, we found no difference in the number of CCT129254-treated and vehicle-treated cells at 0.5, 6, and 24 hours after injection when using a different melanoma cell line 690 (Supplementary Fig. S4).

As we have shown that survival in the blood stream and extravasation are unchanged, we next sought to determine whether the colonization of the lungs is affected by the CCT129254-mediated inhibition of ROCK. We applied an experimental metastasis approach similar to the extravasation assay (see Materials and Methods), using luciferase-expressing 4599 melanoma cells that, after 40 hours of pretreatment with the compounds, were injected into the tail vein of athymic mice and their luminescence measured 24 days after the injection. Importantly, we show that lungs injected with the CCT129254-treated cells exhibit a consistently lower luminescence count than the control or CCT130293-treated cells (Fig. 6B). These results suggest that CCT129254-mediated inhibition of ROCK reduces the ability of the melanoma cells to efficiently grow in the lung. Similar results were found with another melanoma cell line 690 (Supplementary Fig. S5). To strengthen our findings that ROCK signaling is required for outgrowth in the lungs, we used genetic deletion of *Rock1* and *Rock2* in MEFs derived from $Rock1^{fl/fl}/Rock2^{fl/fl}$ embryos (S. Kuemper and C.J. Marshall; unpublished data) that were infected with pBABE-p53DD (37) and pBABE-HRasV12 to generate transformed cell lines (see Materials and Methods). These were then treated in culture with either AdCre to excise the floxed *Rock* alleles, or AdGFP as a control. Using the lung colonization assay, we showed that injection of the *Rock*-deficient MEFs led to a consistently lower number of macroscopic lung metastases than the control transformed MEFs (Fig. 6C), confirming that ROCK activity is needed for efficient colonization of the lung parenchyma.

Discussion

Metastatic spread is responsible for the majority of melanoma-related deaths. The median survival time of patients with metastatic melanoma is 8 to 9 months and the 3-year overall survival rate is less than 15% (38). Despite significant progress made in the last decades, much remains to be discovered about how the metastatic process is initiated and sustained (1), and how to block growth of metastases. As the Rho kinases ROCK1 and ROCK2 have been implicated in cytoskeletal rearrangements involved in cell motility and invasion that are key steps in metastasis, we sought to investigate whether two compounds, CCT129254 and AT13148, which are potent ROCK inhibitors *in vitro* and have good pharmacokinetic properties *in vivo*, would affect metastasis in an *in vivo* melanoma model of spontaneous metastasis.

(*Continued.*) Histograms represent the mean invasion index ± SD from $n = 3$ independent experiments. *, $P < 0.05$; **, $P < 0.01$; ***, $P < 0.001$; ****, $P < 0.0001$, unpaired t test. B, multiphoton intravital imaging of GFP-LifeAct-A375M2 subcutaneous tumors in athymic mice treated with either CCT54 (200 mg/kg) or AT48 (40 mg/kg). Images from the left show A375M2 cells in green and collagen SHG in blue. The right side is an overlay of images 12 minutes apart from a time series colored red, green, and blue to highlight motile cells; white pixels indicate stationary objects. Scale bar, 100 mm. Graphic shows quantification of the number of motile melanoma cells per area of tumor imaged; each dot represents a different field of view. **, $P < 0.001$; ***, $P < 0.0001$, Mann–Whitney U test.

Published OnlineFirst April 3, 2015; DOI: 10.1158/0008-5472.CAN-14-2156

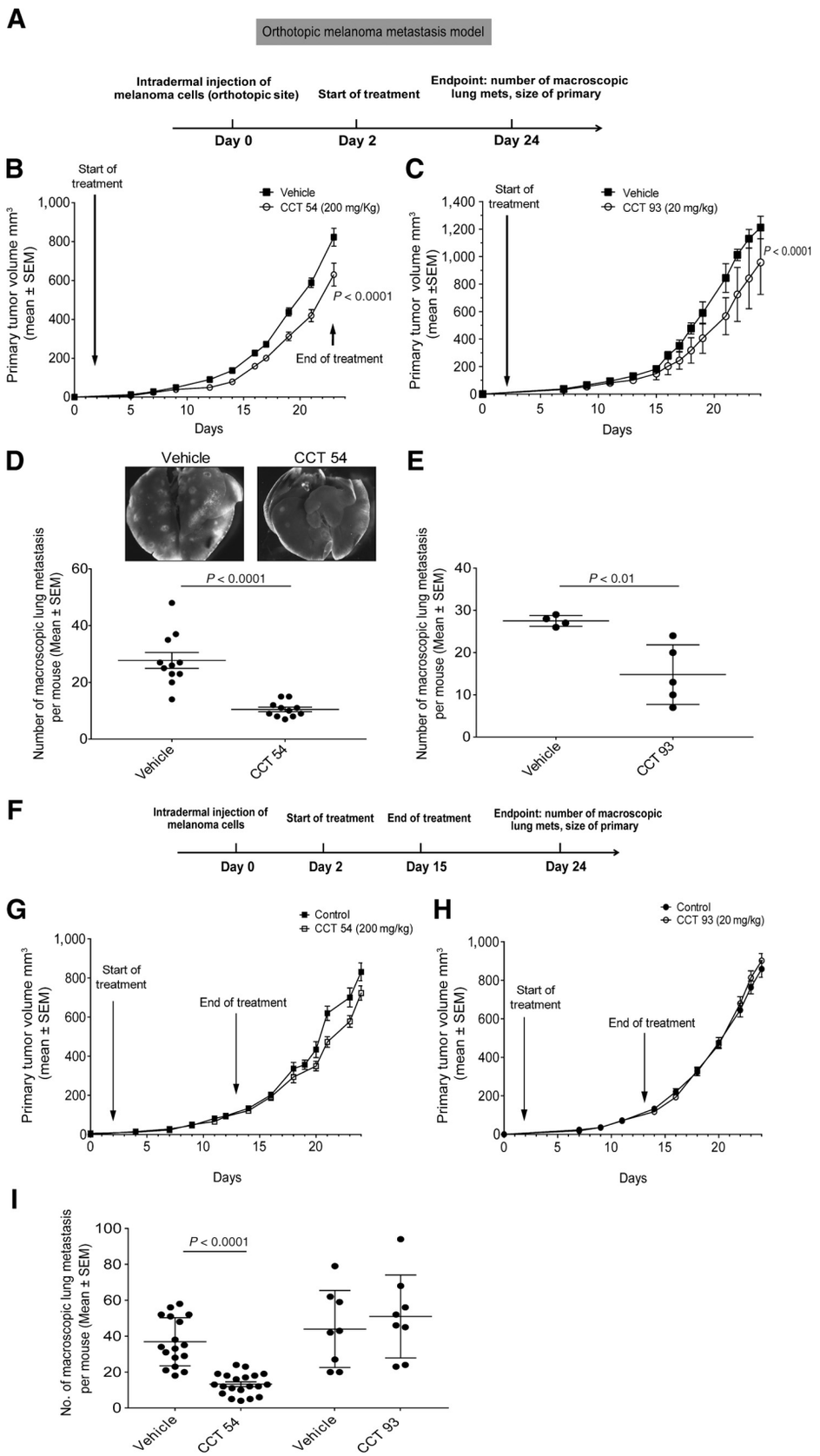

Figure 4.
CCT129254 inhibits spontaneous melanoma metastasis. A, diagram of spontaneous metastasis assay with continuous schedule of drug administration. B and C, graphs show the volume of 4599 primary tumor in NSG mice treated with either CCT54 (200 mg/kg; B) or CCT93 (20 mg/kg; C), for 22 days. $n = 11$ for vehicle- and CCT54-treated mice and $n = 4$ for vehicle- and $n = 5$ for CCT93-treated mice. P value generated with ANOVA. D and E, graphs show number of macroscopic 4599 lung metastases in NSG mice treated with either CCT54 (D) or CCT93 (E) using the continuous schedule. $n = 11$ for vehicle- and CCT54-treated mice and $n = 4$ for vehicle-treated and $n = 5$ for CCT93-treated mice. P value generated with the Student t test. Inset, representative images of macroscopic lung metastases in vehicle- and CCT54-treated mice. F, diagram of the discontinuous schedule. G and H, graphs show the volume of primary tumors treated with either CCT54 (200 mg/kg; G) or CCT93 (20 mg/kg; H), for 14 days. $n = 17$ for vehicle- and CCT54-treated mice and $n = 8$ for vehicle- and CCT93-treated mice. I, graphic shows measurements of the number of macroscopic 4599 lung metastases using the discontinuous schedule. $n = 17$ for vehicle- and CCT54-treated mice and $n = 8$ for vehicle- and CCT93-treated mice, P is generated with a t test. Values, means ± SEM.

Published OnlineFirst April 3, 2015; DOI: 10.1158/0008-5472.CAN-14-2156

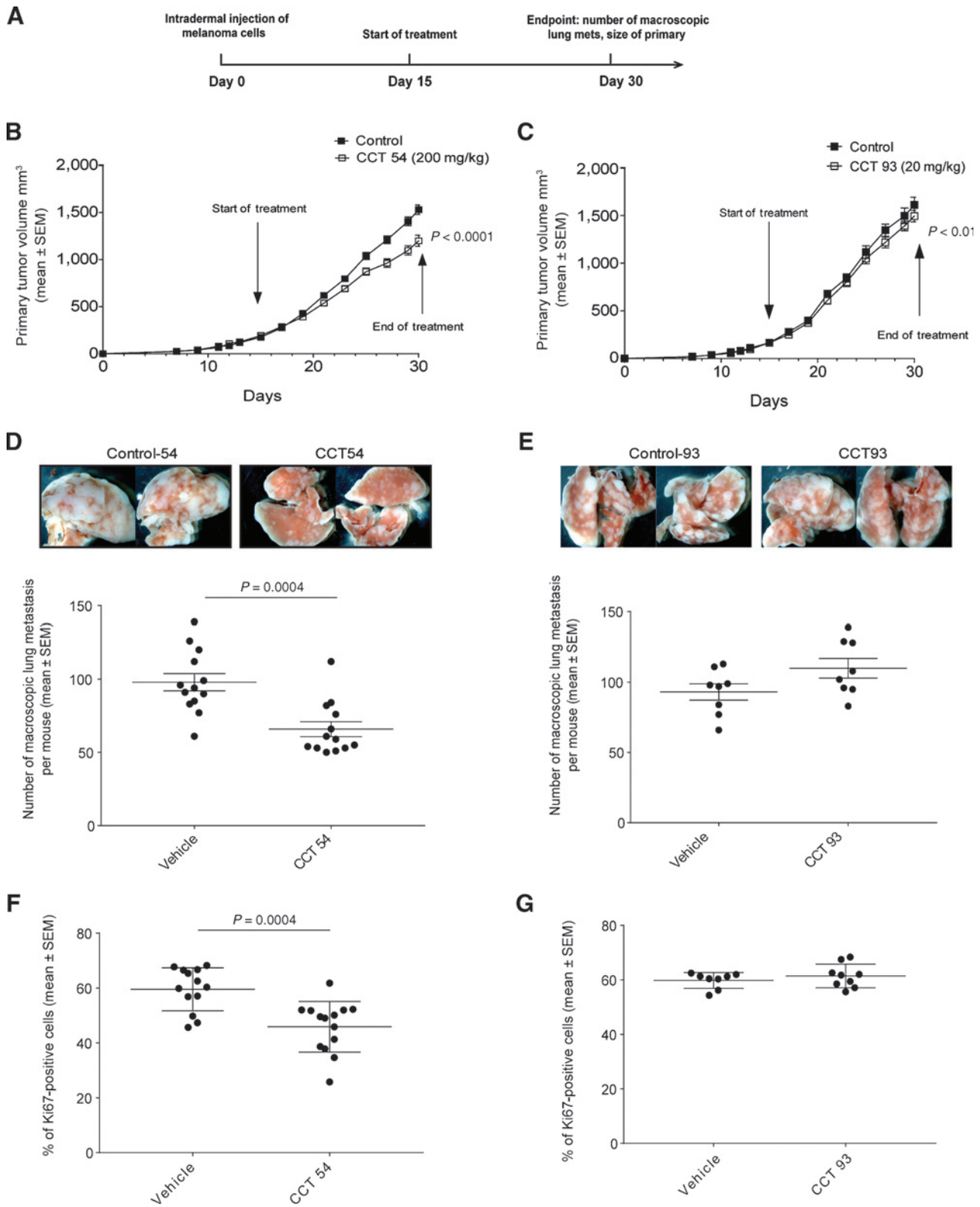

Figure 5.
CCT129254 inhibits the progression of advanced melanoma. A, diagram of the experimental setting. B and C, graphs show the volume of 4599 primary tumor treated with either CCT54 (200 mg/kg; B) or CCT93 (20 mg/kg; C) for 15 days. $n = 13$ for vehicle- and CCT54-treated mice and $n = 8$ for vehicle- and CCT93-treated mice. P is calculated using ANOVA. D and E, graphs show the number of macroscopic lung metastases treated with either CCT54 (D) or CCT93 (E). $n = 13$ for vehicle- and CCT54-treated mice and $n = 8$ for vehicle- and CCT93-treated mice. Insets, representative images of lung macroscopic metastases. F and G, graphs show the percentage of Ki67-positive 4599 melanoma cells in the macroscopic lung metastases from CCT54-treated mice (F) and CCT93-treated mice (G). $n = 13$ for vehicle- and CCT54-treated mice and $n = 8$ for vehicle- and CCT93-treated mice. P is calculated using a t test. Values, means ± SEM.

Published OnlineFirst April 3, 2015; DOI: 10.1158/0008-5472.CAN-14-2156

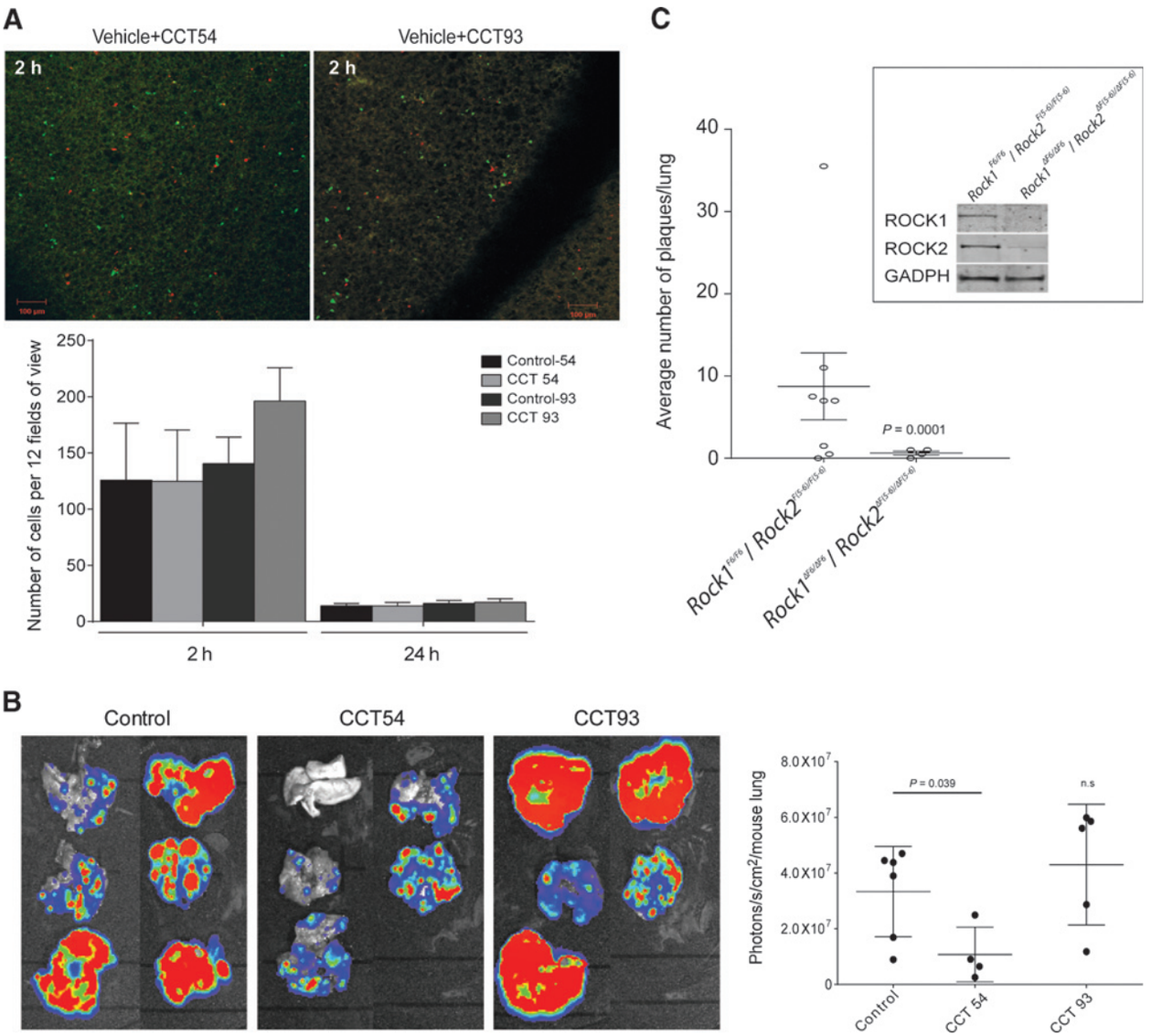

Figure 6.
ROCK inhibition decreases growth of melanoma metastases. A, 4599 cells were labeled with orange or green dye and pretreated with CCT54 (40 μmol/L) or CCT93 (10 μmol/L), mixed with respective control, and injected into the tail vein of athymic mice. Images show lung parenchyma: orange (CCT54- or CCT93-treated) cells and green vehicle-treated cells. Bar, 100 μm. Histograms show the number of vehicle- and drug-treated cells present in 12 fields of view/lung at 2 hours ($n = 3$ animals) and 24 hours ($n = 5$ animals) after injection. B, luciferase-expressing 4599 melanoma cells were pretreated with either CCT54 (40 μmol/L) or CCT93 (10 μmol/L) and injected into the tail vein of athymic mice. Images show lungs 24 days after injection of luminescent 4599 cells. Histogram shows quantification of the luminescence signal. Values are represented by means ± SEM. $n = 6$ mice per condition. P is calculated using a t test. C, graph shows the average number of tumors in lungs 24 days after the tail vein injection of either control (*Rock1*$^{F6/F6}$; *Rock2*$^{F(5\text{-}6)}$/$^{F(5\text{-}6)}$) or recombined (*Rock1*$^{\Delta F6/\Delta F6}$; *Rock2*$^{\Delta F(5\text{-}6)}$/$^{\Delta F(5\text{-}6)}$); *p53*^{DD};*HRas*^{V12}-transformed MEFs. Values, means ± SEM. P is calculated using a t test.

We show that treatment with CCT129254 reduces metastatic load (Fig. 4D and I) even when treatment starts after metastases have been established (Fig. 5D). Importantly, these effects of CCT129254 are mediated by ROCK inhibition as another member of the same chemical series, CCT130293, which does not inhibit ROCK, had limited effects on metastasis in this model (Figs. 4I and 5E). Importantly, we show that both compounds significantly reduce AKT-mediated signaling in the tumors from the treated animals but only CCT129254 consistently inhibited MLC2 phosphorylation (Supplementary Fig. S2). Unfortunately, we were not able to test AT13148 in the spontaneous metastasis model as it proved too toxic to the heavily immunocompromised NSG mice used in these assays. However, we were able to show that both CCT129254 and AT13148 blocked melanoma cell migration *in vivo* as shown by intravital microscopy (Fig. 3B) and cell invasion in a 3D culture model. Significantly, compared with ROCK inhibitors Y27632 and H1152, treatment with CCT129254 and AT13148 blocked both the rounded "amoeboid" and elongated, protrusive mode of cell migration in 3D culture (Fig. 3A). Treatment with ROCK

Published OnlineFirst April 3, 2015; DOI: 10.1158/0008-5472.CAN-14-2156

inhibitors Y27632 or H1152 can induce cells moving in a rounded, "amoeboid" fashion to convert to elongated, protrusive movement (11). Because actomyosin contractility is required for all forms of cell movement on the basis of these results we have previously concluded that other routes to MLC2 phosphorylation such as the CDC42–MRCK pathway can provide the actomyosin contractility for elongated, protrusive movement (10). However, our findings with AT13148 and CCT12954 that do not inhibit MRCK and produce a more sustainable inhibition of ROCK than Y27632 or H1152 show that ROCK is involved in elongated, protrusive movement in some cells. As alternative forms of movement are interconvertible (32), and have been proposed as ways that tumor cells can continue to invade when one mode of movement is blocked (39), the ability of CCT129254 and AT13148 to block both modes of movement is of considerable interest. Strikingly, treatment with CCT129254 or AT13148 led to a collapsed cytoskeletal phenotype (Fig. 2B) like that produced by high doses of the myosin II inhibitor blebbistatin (10), showing that actomyosin contractility was strongly inhibited. This collapsed cytoskeletal morphology was also seen in cells where ROCK1 and ROCK2 had been genetically depleted but not in cells treated with ROCK inhibitors Y27632 or H1152 (Fig. 2B). Because actomyosin contractility is essential for all modes of cell migration (32, 33), it is likely that the pronounced effects of CCT129254 and AT13148 on cell movement are a consequence of their potent inhibition of actomyosin contractility. The *in vitro* kinase screen presented in Supplementary Table S1 revealed that in addition to the inhibition of ROCK, CCT129254 exhibits a high potency toward the inhibition of S6K1, AKT1, PKA, and MSK, and although we show that CCT130293, which exhibits a very similar inhibitory profile to CCT129254 but does not inhibit ROCK, does not affect any of the actomyosin contractility-driven processes, the influence of inhibition of these additional kinases on the *in vitro* and *in vivo* phenotypes cannot be entirely discarded.

Extravasation of circulating tumor cells from the blood stream into distant tissues is an essential step in metastasis. We found that CCT129254 treatment did not affect the ability of cells to lodge in the lung; however, outgrowth to form tumor nodules was affected (Fig. 6B). Treatment with CCT130293, which does not inhibit ROCK, had no effect on the outgrowth of extravasated cells. This result argues that proliferation at the secondary site requires ROCK. To gain further support for this idea, we genetically deleted *Rock1* and *2* from MEFs transformed by mutant *p53* and $HRAS^{V12}$ such cells failed to grow in the lung, after tail vein injection (Fig. 6C). Growth of disseminated tumor cells at secondary sites requires cell proliferation. Strikingly, we found that CCT129254 treatment led to inhibition of proliferation in metastases (Fig. 5F), whereas treatment with CCT130293 did not. This inhibition of proliferation may reflect a direct requirement for ROCK in cell proliferation that has been seen in some cell types (40, 41) but not all (42). Interestingly, as demonstrated by Sahai and colleagues (42), the dependence of cells on ROCK may be context-dependent as Ras-transformed fibroblasts do not require ROCK signaling for proliferation when cultured under anchorage-dependent conditions, but do in anchorage-independent conditions. However, the role of ROCK in tumor proliferation may be indirect as Samuel and colleagues (4) have shown that ROCK-dependent remodeling of the extracellular matrix can enhance cell proliferation through stimulation of β-catenin signaling. Thus, a requirement for ROCK signaling in cell proliferation may only be seen in situations in which there is dependence on the tumor microenvironment.

In conclusion, we show that two new ROCK inhibitors AT13148 and CCT129254 potently inhibit ROCK-mediated functions in melanoma cells. We show that inhibition of ROCK by CCT129254 impairs the migration of cells in tumors and the growth of melanoma cells in the lungs. Importantly, we show that CCT129254 treatment reduced the growth of established metastases arguing that the effects of CCT129254 are not just mediated by effects on cell migration from the primary tumor. We show that the effects we observe on inhibition of cell proliferation in metastases by CCT129254 require ROCK inhibition, which suggests that such compounds may be useful in treating metastatic disease.

Disclosure of Potential Conflicts of Interest

J. Caldwell has provided expert testimony for The Institute of Cancer Research that operates Rewards to Inventors Scheme, covering compounds used in this article. I. Collins has provided expert testimony for the Institute of Cancer Research Awards to Inventors Scheme—payments related to licensing of the chemical matter related to that described in this article. M.D. Garrett is a consultant/advisory board member for Astex Pharmaceuticals and has provided expert testimony for Cancer Research UK. No potential conflicts of interest were disclosed by the other authors.

Authors' Contributions

Conception and design: A. Sadok, M.D. Garrett, C.J. Marshall
Development of methodology: A. Sadok, F.K. Mardakheh, C.J. Marshall
Acquisition of data (provided animals, acquired and managed patients, provided facilities, etc.): A. Sadok, A. McCarthy, I. Collins, S. Hooper, E. Sahai, S. Kuemper, F.K. Mardakheh
Analysis and interpretation of data (e.g., statistical analysis, biostatistics, computational analysis): A. Sadok, A. McCarthy, E. Sahai, S. Kuemper, C.J. Marshall
Writing, review, and/or revision of the manuscript: A. Sadok, I. Collins, M.D. Garrett, S. Kuemper, C.J. Marshall
Administrative, technical, or material support (i.e., reporting or organizing data, constructing databases): J. Caldwell, M. Yeo
Study supervision: A. Sadok, C.J. Marshall
Other (selection and provision of chemical tools for study): I. Collins
Other (provided access to compounds and accompanying resources; discussions on conception and design of parts of the study): M.D. Garrett

Acknowledgments

The authors thank R. Marais (Paterson Institute, Manchester, United Kingdom) and R. Hynes (MIT, Cambridge, MA) for melanoma cell lines. The authors also thank G. Damoulakis for helpful comments on the article and all other members of the Marshall laboratory for their comments and discussions.

Grant Support

This work was financially supported by Cancer Research UK [grant numbers C107/A10433 and C107/A104339 (C.J. Marshall); C309/A11566 (M.D. Garrett, J. Caldwell, and I. Collins)] and a Marie Curie Intra-European Fellowship to A. Sadok. C.J. Marshall is a Gibb Life Fellow of CRUK.

The costs of publication of this article were defrayed in part by the payment of page charges. This article must therefore be hereby marked *advertisement* in accordance with 18 U.S.C. Section 1734 solely to indicate this fact.

Received July 23, 2014; revised February 7, 2015; accepted February 23, 2015; published OnlineFirst April 3, 2015.

References

1. Vanharanta S, Massague J. Origins of metastatic traits. Cancer Cell 2013;24:410–21.
2. Hall A. Rho family GTPases. Biochem Soc Trans 2012;40:1378–82.
3. Rath N, Olson MF. Rho-associated kinases in tumorigenesis: re-considering ROCK inhibition for cancer therapy. EMBO Rep 2012;13:900–8.
4. Samuel MS, Lopez JI, McGhee EJ, Croft DR, Strachan D, Timpson P, et al. Actomyosin-mediated cellular tension drives increased tissue stiffness and beta-catenin activation to induce epidermal hyperplasia and tumor growth. Cancer Cell 2011;19:776–91.
5. Butcher DT, Alliston T, Weaver VM. A tense situation: forcing tumour progression. Nat Rev Cancer 2009;9:108–22.
6. Mueller BK, Mack H, Teusch N. Rho kinase, a promising drug target for neurological disorders. Nat Rev Drug Discov 2005;4:387–98.
7. Riento K, Ridley AJ. Rocks: multifunctional kinases in cell behaviour. Nat Rev Mol Cell Biol 2003;4:446–56.
8. Sahai E, Marshall CJ. Differing modes of tumour cell invasion have distinct requirements for Rho/ROCK signalling and extracellular proteolysis. Nat Cell Biol 2003;5:711–9.
9. Olson MF, Sahai E. The actin cytoskeleton in cancer cell motility. Clin Exp Metastasis 2009;26:273–87.
10. Wilkinson S, Paterson HF, Marshall CJ. Cdc42-MRCK and Rho-ROCK signalling cooperate in myosin phosphorylation and cell invasion. Nat Cell Biol 2005;7:255–61.
11. Sanz-Moreno V, Gadea G, Ahn J, Paterson H, Marra P, Pinner S, et al. Rac activation and inactivation control plasticity of tumor cell movement. Cell 2008;135:510–23.
12. Uehata M, Ishizaki T, Satoh H, Ono T, Kawahara T, Morishita T, et al. Calcium sensitization of smooth muscle mediated by a Rho-associated protein kinase in hypertension. Nature 1997;389:990–4.
13. Sasaki Y, Suzuki M, Hidaka H. The novel and specific Rho-kinase inhibitor (S)-(+)-2-methyl-1-[(4-methyl-5-isoquinoline)sulfonyl]-homopiperazine as a probing molecule for Rho-kinase-involved pathway. Pharmacol Ther 2002;93:225–32.
14. Vigil D, Kim TY, Plachco A, Garton AJ, Castaldo L, Pachter JA, et al. ROCK1 and ROCK2 are required for non–small cell lung cancer anchorage-independent growth and invasion. Cancer Res 2012;72:5338–47.
15. Patel RA, Liu Y, Wang B, Li R, Sebti SM. Identification of novel ROCK inhibitors with anti-migratory and anti-invasive activities. Oncogene 2014;33:550–5.
16. McHardy T, Caldwell JJ, Cheung KM, Hunter LJ, Taylor K, Rowlands M, et al. Discovery of 4-amino-1-(7H-pyrrolo[2,3-d]pyrimidin-4-yl)piperidine-4-carboxamides as selective, orally active inhibitors of protein kinase B (Akt). J Med Chem 2010;53:2239–49.
17. Yap TA, Walton MI, Grimshaw KM, Te Poele RH, Eve PD, Valenti MR, et al. AT13148 is a novel, oral multi-AGC kinase inhibitor with potent pharmacodynamic and antitumor activity. Clin Cancer Res 2012;18:3912–23.
18. Gadea G, Sanz-Moreno V, Self A, Godi A, Marshall CJ. DOCK10-mediated Cdc42 activation is necessary for amoeboid invasion of melanoma cells. Curr Biol 2008;18:1456–65.
19. Sanz-Moreno V, Gaggioli C, Yeo M, Albrengues J, Wallberg F, Viros A, et al. ROCK and JAK1 signaling cooperate to control actomyosin contractility in tumor cells and stroma. Cancer Cell 2011;20:229–45.
20. Nikolaou VA, Stratigos AJ, Flaherty KT, Tsao H. Melanoma: new insights and new therapies. J Invest Dermatol 2012;132:854–63.
21. Bis S, Tsao H. Melanoma genetics: the other side. Clin Dermatol 2013;31:148–55.
22. Homet B, Ribas A. New drug targets in metastatic melanoma. J Pathol 2014;232:134–41.
23. Finn L, Markovic SN, Joseph RW. Therapy for metastatic melanoma: the past, present, and future. BMC Med 2012;10:23.
24. Dhomen N, Reis-Filho JS, da Rocha Dias S, Hayward R, Savage K, Delmas V, et al. Oncogenic Braf induces melanocyte senescence and melanoma in mice. Cancer Cell 2009;15:294–303.
25. Wyckoff JB, Pinner SE, Gschmeissner S, Condeelis JS, Sahai E. ROCK- and myosin-dependent matrix deformation enables protease-independent tumor-cell invasion *in vivo*. Curr Biol 2006;16:1515–23.
26. Malanchi I, Santamaria-Martinez A, Susanto E, Peng H, Lehr HA, Delaloye JF, et al. Interactions between cancer stem cells and their niche govern metastatic colonization. Nature 2012;481:85–9.
27. Saxty G, Woodhead SJ, Berdini V, Davies TG, Verdonk ML, Wyatt PG, et al. Identification of inhibitors of protein kinase B using fragment-based lead discovery. J Med Chem 2007;50:2293–6.
28. Lin K, Lin J, Wu WI, Ballard J, Lee BB, Gloor SL, et al. An ATP-site on-off switch that restricts phosphatase accessibility of Akt. Sci Signal 2012;5:ra37.
29. Yap TA, Yan L, Patnaik A, Fearen I, Olmos D, Papadopoulos K, et al. First-in-man clinical trial of the oral pan-AKT inhibitor MK-2206 in patients with advanced solid tumors. J Clin Oncol 2011;29:4688–95.
30. Hooper S, Gaggioli C, Sahai E. A chemical biology screen reveals a role for Rab21-mediated control of actomyosin contractility in fibroblast-driven cancer invasion. Br J Cancer 2010;102:392–402.
31. Straight AF, Cheung A, Limouze J, Chen I, Westwood NJ, Sellers JR, et al. Dissecting temporal and spatial control of cytokinesis with a myosin II Inhibitor. Science 2003;299:1743–7.
32. Sanz-Moreno V, Marshall CJ. The plasticity of cytoskeletal dynamics underlying neoplastic cell migration. Curr Opin Cell Biology 2010;22:690–6.
33. Friedl P, Wolf K. Plasticity of cell migration: a multiscale tuning model. J Cell Biol 2010;188:11–9.
34. Yin Z, Sadok A, Sailem H, McCarthy A, Xia X, Li F, et al. A screen for morphological complexity identifies regulators of switch-like transitions between discrete cell shapes. Nat Cell Biol 2013;15:860–71.
35. Pinner S, Sahai E. Imaging amoeboid cancer cell motility *in vivo*. J Microsc 2008;231:441–5.
36. Pinner S, Jordan P, Sharrock K, Bazley L, Collinson L, Marais R, et al. Intravital imaging reveals transient changes in pigment production and Brn2 expression during metastatic melanoma dissemination. Cancer Res 2009;69:7969–77.
37. Shaulian E, Zauberman A, Ginsberg D, Oren M. Identification of a minimal transforming domain of p53: negative dominance through abrogation of sequence-specific DNA binding. Mol Cell Biol 1992;12:5581–92.
38. Balch CM, Gershenwald JE, Soong SJ, Thompson JF, Atkins MB, Byrd DR, et al. Final version of 2009 AJCC melanoma staging and classification. J Clin Oncol 2009;27:6199–206.
39. Wolf K, Friedl P. Molecular mechanisms of cancer cell invasion and plasticity. Br J Dermatol 2006;154(Suppl 1):11–5.
40. Sauzeau V, Le Mellionnec E, Bertoglio J, Scalbert E, Pacaud P, Loirand G. Human urotensin II-induced contraction and arterial smooth muscle cell proliferation are mediated by RhoA and Rho-kinase. Circ Res 2001;88:1102–4.
41. Tharaux PL, Bukoski RC, Rocha PN, Crowley SD, Ruiz P, Nataraj C, et al. Rho kinase promotes alloimmune responses by regulating the proliferation and structure of T cells. J Immunol 2003;171:96–105.
42. Sahai E, Ishizaki T, Narumiya S, Treisman R. Transformation mediated by RhoA requires activity of ROCK kinases. Curr Biol 1999;9:136–45.

Published OnlineFirst April 3, 2015; DOI: 10.1158/0008-5472.CAN-14-2156

Cancer Research
The Journal of Cancer Research (1916–1930) | The American Journal of Cancer (1931–1940)

AACR American Association for Cancer Research

Rho Kinase Inhibitors Block Melanoma Cell Migration and Inhibit Metastasis

Amine Sadok, Afshan McCarthy, John Caldwell, et al.

Cancer Res 2015;75:2272-2284. Published OnlineFirst April 3, 2015.